Journal of Alloys and Compounds 508 (2010) 309–314

Contents lists available at ScienceDirect

Journal of Alloys and Compounds

journal homepage: www.elsevier.com/locate/jallcom

A revision of the Sm-rich region of the Sm–Co system

Y. Yuan[a,b], S. Delsante[a], J. Yi[b], G. Borzone[a,*]

[a] Department of Chemistry and Industrial Chemistry, University of Genoa, INSTM UdR Genoa, Via Dodecaneso 31, I- 16146 - Genoa, Italy
[b] State Key Laboratory of Powder Metallurgy, Central South University, Changsha, Hunan 410083, PR China

ARTICLE INFO

Article history:
Received 9 June 2010
Accepted 8 August 2010
Available online 19 August 2010

Keywords:
Sm–Co phase diagram
Rare-earth alloys and compounds
Thermal analysis
Scanning electron microscopy

ABSTRACT

The Sm-rich side of the Sm–Co system has been experimentally reinvestigated using the differential scanning calorimetry (DSC) method with slow rates of 1 °C/min and 0.5 °C/min as well as microscope and X-ray diffraction (XRD) analyses. Combining the experimental results from DSC, XRD and EPMA (Electron Probe MicroAnalysis) analyses, five invariant reactions have been determined and the existence of the Sm_3Co and Sm_5Co_2 phases confirmed. The phase diagram of Sm–Co system has been accordingly modified.

1. Introduction

The permanent magnetic materials based on rare-earth intermetallic compounds have excellent magnetic properties such as high remanence and high maximum energy product. [1,2]. Among these, the widely used magnets are made up of representative constituents $Sm(Co,Cu,Fe,Zr)_x$, and characterized by a continuous cellular precipitation microstructure consisting of $Sm(Co,Cu)_5$ and $Sm_2(Co,Fe)_{17}$ [3,4]. The magnetic properties of this series of alloys are associated with the composition of each phase, the ratio between 1:5 and 2:17 type phases, and details of the cellular structure. Therefore, it is important to obtain information on the relevant phase diagrams and here we have focused on the Sm–Co system.

The Sm–Co system has attracted much attention [5–15] for the excellent magnetic properties of the Co-rich alloys. The most recent experimental study of the Sm–Co system was carried out by Ge et al. [5]. They mainly concentrated on the Co-rich portion and their version is similar to that previously proposed by Buschow and van der Goot [8,9]; they also confirmed the existence of Sm_5Co_{19} and, in the case of $SmCo_5$, only as a high temperature phase which undergoes to decomposition. According to the information from literature, the phase diagram on the Co-rich side of the Sm–Co system seems to be fairly well established [7,15]. However, some uncertainty still remains on the Sm-rich side.

Moreau and Paccard [13] pointed out that the Sm_9Co_4 (30.8 at.% Co) phase should be replaced by the Sm_5Co_2 (28.6 at.% Co) phase with a mS28-Mn_5C_2 structure type. Moreover, the temperature 670 °C of the eutectic reaction $L \leftrightarrow Sm + Sm_3Co$ determined by Ge et al. [5] is much higher than the 595 °C determined by Buschow and van der Goot [8,9], although both carried out DSC analysis using alumina crucible.

Therefore the Sm-rich side of the Sm–Co system needs revision and is the subject of this work.

2. Experimental

All the alloys were prepared from elements with a purity of 99.9 mass% (Sm) and 99.98+ mass% (Co). The samples, pellets of the finely mixed metal powders or pieces of the metals, were enclosed in a gas-tight tantalum crucible sealed by arc-welding under an argon atmosphere, and melted in an induction furnace. The temperature was increased and controlled with the aim of avoiding any possible reaction between Ta and Co.

The alloy buttons were divided into three pieces. One piece of about 500–700 mg was sealed under an argon atmosphere in Ta crucible for differential scanning calorimetry (DSC) analysis with two cycles from 350 to 820 °C with heating and cooling rates of 1 °C/min, followed by a 2nd run at 0.5 °C/min. An empty Ta crucible of the same weight as the Ta crucible holding the sample was used as a reference.

The DSC111 SETARAM apparatus designed as a Calvet calorimeter (where the cylindrical reference and working cells are surrounded by two differentially connected thermal fluximeters) was used in a continuous mode. The calorimeter was calibrated by measuring the melting temperature (T_m) of metallic In, Sn, Pb and Zn (99.999 mass% purity) and the temperature was obtained with an accuracy of $T_m \pm 0.5$ °C.

For selected alloys the remaining portions of ingots were put in an Al_2O_3 crucible, sealed under argon atmosphere in quartz tubes and subjected to heat treatment at 540 °C for 54 days and 620 °C for 20 days respectively, and then quenched in icy water. Several alloys were also annealed at 500 °C for 45 days and quenched in the same way.

After DSC measurements and annealing treatments, microstructural observation by light optical microscopy (LOM), scanning electron microscopy (SEM) and chemical analysis by energy dispersive X-ray spectroscopy (EDXS) was carried out on polished specimens. A Leica Digital Microscope and a Zeiss EVO 40 SEM (Carl Zeiss SMT Ltd., Cambridge) operating at 20 kV, equipped with an INCA 300 Electron Probe MicroAnalysis (EPMA) were employed.

* Corresponding author. Tel.: +39 010 3536153, fax: +39 010 3625051.
E-mail address: gabriella.borzone@unige.it (G. Borzone).

0925-8388/$ – see front matter © 2010 Published by Elsevier B.V.
doi:10.1016/j.jallcom.2010.08.035

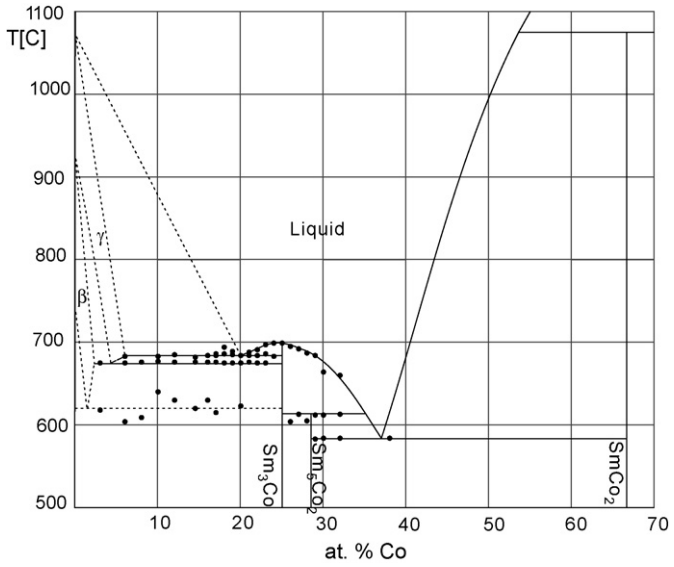

Fig. 1. Experimental phase diagram of the Sm–Co system in the Sm-rich region. The points marked are taken from the heating run, see text.

Selected powder specimens have been investigated by XRD analysis performed using a Philips *X'Pert MPD* machine (Philips, Almeno, The Netherlands) equipped with a copper target, excited to 40 kV and 30 mA, and a solid state detector. This analysis was used both for phase identification and for lattice parameter measurements. The lattice parameters were refined by least-squares fit, using the Nelson–Riley function.

3. Results and discussion

3.1. Differential scanning calorimetry results

The Sm-rich portion of the Sm–Co phase diagram has been modified on the basis of the DSC results and is shown in Fig. 1. The DSC analysis data are summarized in Table 1 and the temperature assigned to the five invariant reactions identified in this work is reported in Table 2. Generally, the temperature values reported here are taken from the second DSC run at a rate of 0.5 °C/min, except for the temperature of reaction e_3 which is taken from the first cycle at the rate of 1 °C/min. On heating, the onset temperature of the thermal effect was selected as the temperature of the invariant reaction and, for alloys with Co content >20 at.%, the peak temperature of the last thermal event as the liquidus temperature [16]. Because of the limited temperature range in which the DSC instrument can work, the liquidus temperature of the alloys with Co < 20 at.% has not been detected.

For the samples containing Sm together with the Sm_3Co phase, the DSC curves obtained in the two cycles and related to the invariant reactions e_1 and e_2 coincide. The thermal effect corresponding to the invariant reaction e_3 which only appeared in the first heating process, and which disappeared in the following process due to the effect of hydrogen, will be discussed later.

The temperature of the e_4 and p_1 invariant reactions is in fairly good agreement with that reported by [5,8]. Some examples of the DSC curves for as-cast samples obtained at different heating rates are shown in Fig. 2a–c. From Fig. 2a it is obvious the congruent melting of the Sm_3Co phase.

3.2. The effect of crucibles

Because of the high reactivity of the rare-earth metals, especially in a liquid state, the contamination from the crucible cannot be completely eliminated. Tungsten and tantalum crucibles are considered to be the best because they do not react with the molten

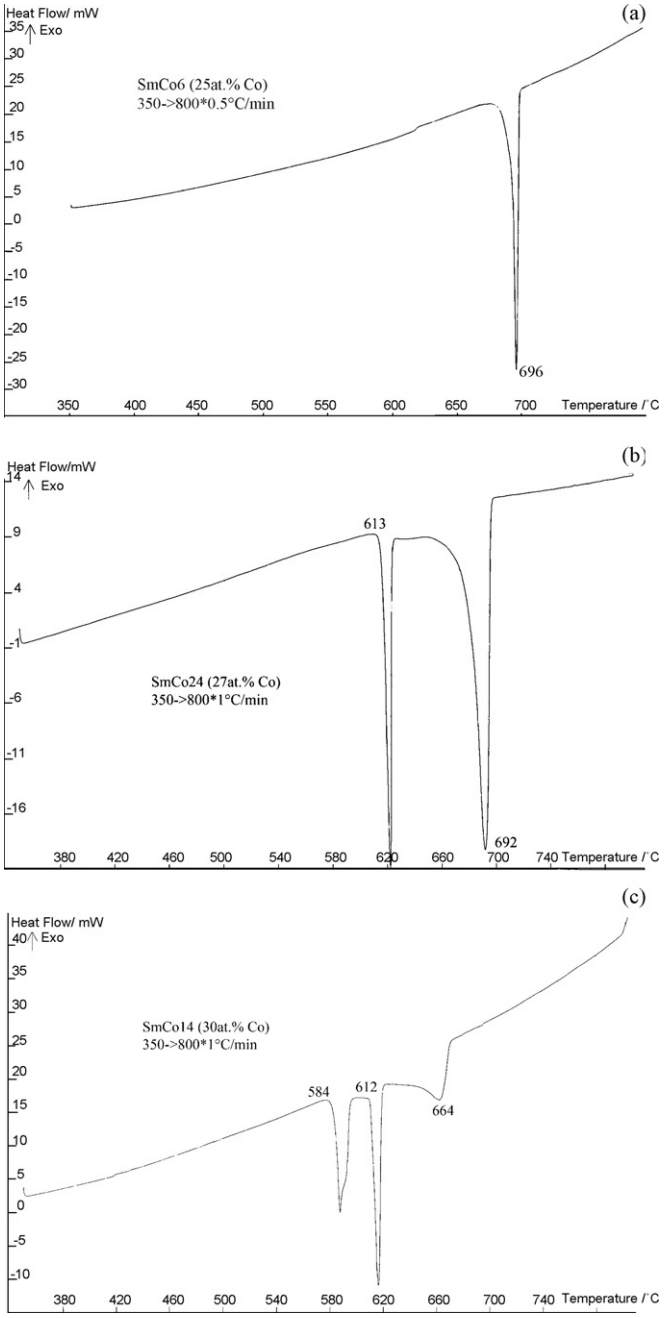

Fig. 2. (a–c) Examples of the DSC heating curves of Sm–Co alloys processed in Ta crucibles.

rare-earth metals at temperatures below 1000 °C. van der Goot and Buschow [8] and Ge et al. [5], both used alumina crucible for DTA measurements. We also used alumina crucibles at first, but we observed the formation of a small quantity of Sm–Al–Co ternary phase. A BN crucible was then tried out, but was also found to be unsuitable because of the reaction with the metals. Therefore, Ta crucibles were used. As the samples investigated belong to the Sm-rich side, the reaction between Ta and Co can be disregarded.

For all the samples having a composition < 25 at.% Co, the DSC results for the 2nd run showed systematically a small peak at around 450 °C, which did not exist in the first heating run. This can be correlated to the partial reaction of Sm with hydrogen as observed by Leon-Escamilla and Corbett who highlighted that Ta becomes permeable to H_2 above 600 °C [17]. Thus, in the 2nd heating run of DSC analysis, despite the argon flux, Sm was thought

Table 1
Experimental results of DSC (°C) and SEM–EDS compositions of the investigated Sm–Co alloys.

Sample	at.% Co	1st heating 1 °C/min	1st cooling	2nd heating 0.5 °C/min	2nd cooling	Reaction
N.23	3	618				
		675	672	675	671	e_2
N.11	6	604		600		
		675	675	675	675	e_2
		683		683	680	
N. 12	8	610				
		676	672	675	675	e_2
N. 7	10	640		640		
		677	677	677	677	e_2
		683		684	680	e_1
N. 8	12	633		640		
		676	676	676		e_2
		686	681	685	684	e_1
N. 16	14.5	620				
		676	672	676	673	e_2
		682		680		e_1
N. 22	16	634		630	620	
		676	674	676	676	e_2
		684	679	684	680	e_1
N. 20	17	613		615		
		676	673	675	676	e_2
		684	677	683	679	e_1
N. 9	18	675	675	675	676	e_2
		686	683	684	683	e_1
		690	684	694	688	Liquidus
N. 17	19	675	674	675	676	e_2
		685	678	685	678	e_1
		686	679	689	683	Liquidus
N. 10	20	623				
		675	673	676	676	e_2
		685	679	684	678	e_1
N. 4	21	671	676	675		e_2
		682	680	684	678	e_1
		689	681	689	684	Liquidus
N. 18	22	676	675	674	675	e_2
		684	677	684	677	e_1
		691	679	689	679	Liquidus
N. 19	23	676	677	675	677	e_2
		684		686	683	e_1
		699	690	697	689	Liquidus
N. 5	24	684	680	686	680	e_1
		700	693	697	690	Liquidus
N. 6	25	699	687	696	690	Liquidus
N. 3	26	604	608	608	606	p_1
		693	687	695	688	Liquidus
N. 24	27	613	617	613	614	p_1
		692	690	695	690	Liquidus
N. 13	28	606	613	606	610	p_1
		687	686	688	687	Liquidus
N. 25	29	583	577	584	578	e_4
		615	618	614	615	p_1
		684	682	682	677	Liquidus
N. 14	30	584	579	580	580	e_4
		612	614	605	612	p_1
		664	664	667	665	Liquidus
N. 15	32	586	579	583	583	e_4
		613	615	603	615	p_1
		659	654	660	657	Liquidus
N. 29	38			584	583	e_4
					585	Liquidus

e: Eutectic reaction
p: Peritectic reaction

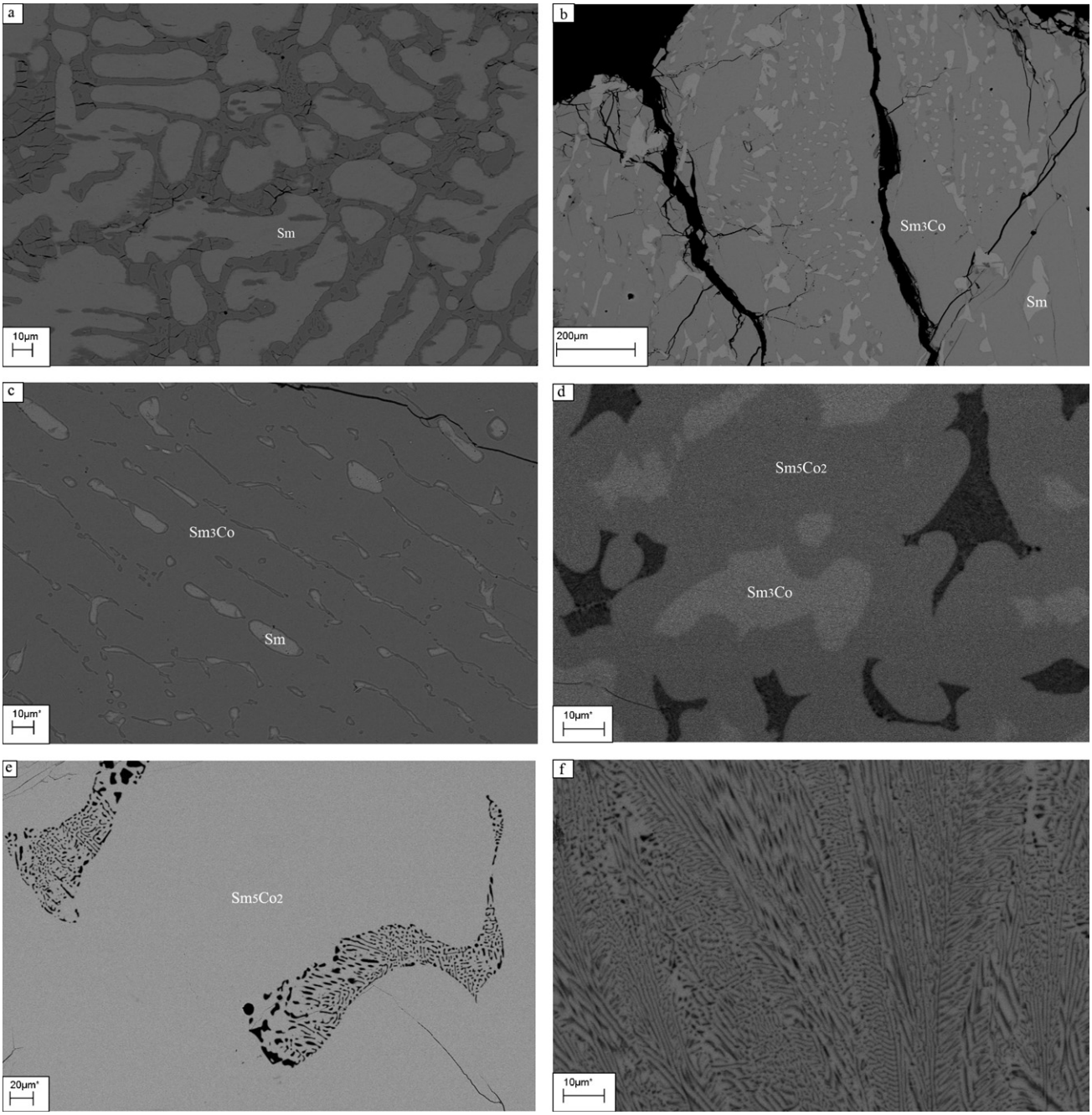

Fig. 3. (a–f) Micrographic aspect of selected Sm–Co samples: (a) alloy Sm–8Co as-cast, white phase (Sm) and (Sm + Sm_3Co) eutectic mixture; (b) alloy Sm–20Co after DSC, white phase (Sm_3Co) and (Sm + Sm_3Co) eutectic mixture; (c) alloy Sm–22Co annealed at 500 °C for 45 days and quenched in icy water, light grey phase (Sm) and Sm_3Co (dark grey phase); (d) alloy Sm–27Co as-cast, light grey phase (Sm_3Co), dark grey phase (Sm_5Co_2 with peritectic formation) and Sm_5Co_2–$SmCo_2$ eutectic mixture; (e) alloy Sm–29Co after DSC, light grey phase Sm_5Co_2 crystals and eutectic mixture (Sm_5Co_2 + $SmCo_2$); (f) alloy Sm–38Co eutectic mixture of (Sm_5Co_2 + $SmCo_2$).

to absorb hydrogen. In order to clarify this, pure Sm sealed in Ta crucible was subjected to the same DSC procedure.

In the first run, on heating, only a small effect at 735 °C was observed. However, on cooling, a peak appeared at 435 °C.

XRD analysis carried out on the sample after DSC showed the presence of α(Sm) and the remaining diffraction lines could be indexed as SmH_2. Considering the Sm–H phase diagram [18], the weak thermal effect at around 450 °C observed in the 2nd DSC measurement on heating was therefore due to the reaction β(Sm)(solid solution) ↔ α(Sm) + SmH_2. This observation is in agreement with the findings of Beaudry and Gschneidner [19] who reported that hydrogen has in fact a pronounced effect on the β-Sm and the α ↔ β transformation is lowered from 731 °C to 430 °C, stabilizing the β-Sm phase over the α-Sm allotrope.

A further confirmation of these assumptions was obtained by using the only two Mo crucibles at our disposal at the time. Sm and Co powders with a composition of 16 at.% Co were sealed in the larger Mo crucible and synthesised by induction melting. One piece of ingot was sealed in the smaller Mo crucible and investigated by DSC in the 400–800 °C temperature range with a rate of 0.3 °C/min. Three effects were recorded on heating at 620, 674 and 683 °C and two effects on cooling at 677 and 676 °C. No thermal effect was observed at 450 °C.

These considerations allowed us to disregard the effect at 450 °C and to assign to the reaction β(Sm) ↔ α(Sm) + Sm_3Co the thermal

Table 2
Invariant reactions in the Sm–Co system determined in this work in comparison with literature data.

Type	Invariant reaction	T (°C) This work	T (°C) [8]	T (°C) [5]
e_1	Liquid ↔ γ(Sm) + Sm_3Co	685		
	Liquid ↔ (Sm) + Sm_3Co		595	670
e_2	γ(Sm) ↔ β(Sm) + Sm_3Co	675	–	–
e_3	β(Sm) ↔ α(Sm) + Sm_3Co	~620	–	–
	Liquid ↔ Sm_3Co	696	695	700
p_1	Liquid + Sm_3Co ↔ Sm_5Co_2	613	605	613
e_4	Liquid ↔ Sm_5Co_2 + $SmCo_2$	583	575	590

Table 3
Crystallographic data in the Sm-rich region of the Sm–Co system.

Phase	Type structure	Lattice parameters (Å)					Refs. and remarks
		a	b	c	Beta	V (Å^3)	
γ-Sm	cP2-W	–	–	–	–	–	[20]
β-Sm	hP2-Mg	3.663	3.663	5.845		67.9	[21]
α-Sm	hR9-Sm	3.629	3.629	26.21		298.9	[22]
α-Sm	hR9-Sm	3.627	3.627	26.19		298.4	T.W., alloy N.23 (3 at.% Co) annealed 54 days at 540 °C
Sm_3Co	oP16-Fe_3C	7.055	9.605	6.342		429.8	[23]
Sm_3Co	oP16-Fe_3C	7.049	9.605	6.336		429.0	T.W., alloy N.18 (22 at.% Co) annealed 45 days at 500 °C
Sm_3Co	oP16-Fe_3C	7.052	9.605	6.339		429.4	T.W., alloy N.6 (25 at.% Co) annealed 20 days at 620 °C
Sm_5Co_2	mS28-Mn_5C_2	16.282	6.392	7.061	96.6	730.0	[13]
Sm_5Co_2	mS28-Mn_5C_2	16.220	6.411	7.032	96.6	726.4	T.W., alloy N.25 (29 at.% Co) annealed 20 days at 620 °C
$SmCo_2$	cF24-$MgCu_2$	7.260	7.260	7.260		382.7	[8]
SmH_2	cF12-CaF_2	5.370	5.3704	5.3704		154.9	[24]
SmH_2	cF12-CaF_2	5.368	5.368	5.368		154.7	T.W., alloy N.23 (3 at.% Co) after DSC

T.W. = this work

effect at around 620 °C observed in the first run of the DSC measurements in the (Sm–Sm_3Co) two-phase field alloys.

3.3. XRD and metallographic analysis

The XRD results are summarized in Table 3 and are consistent with crystal structure literature data [8,13,20–24] available for the Sm–Co phases in the Sm-rich region.

The X-ray diffraction results obtained for the Sm_3Co in samples belonging to the Sm–Sm_3Co two-phase region pointed to a negligible homogeneity field.

The X-ray diffraction pattern obtained for the sample at 28.5 at.% Co was indexed as mS28-Mn_5C_2 with lattice parameters in good agreement with those reported for Sm_5Co_2 by Moreau and Paccard [13]. The phase Sm_9Co_4 reported by van der Goot and Buschow [8] and Ge et al. [5] with 30.8 at.% Co and orthorhombic structure was not found in this work.

As far as the alloys richest in samarium are concerned, no definite indication was obtained from the EPMA analysis for the Co solubility in α-Sm which was close to zero, below the margin of error for the instrument used. On samples annealed at 620 °C for 20 days, the Co solubility observed in β(Sm) is about 1.3 at.% Co.

According to the EPMA analyses of the different samples after DSC, the eutectic composition of the reaction e_1 is around 20.0 at.% Co and of the reaction e_4 is 37 at.% Co, which agree very well with the thermal effects recorded, the microstructure observed and the literature data.

Selected microphotographs of the analysed alloys using the Backscattered electrons (BSE) signal are reported in Fig. 3(a–f).

Fig. 3a shows the BSE image of the as-cast Sm–8Co with primary Sm crystals surrounded by the Sm–Sm_3Co eutectic mixture. Primary crystallization consistent with the liquidus curve was tested by metallographic investigation of selected samples after DSC measurements. As an example, crystals of Sm_3Co and β(Sm)–Sm_3Co eutectic mixture is shown in Fig. 3b in a sample with the Sm–20Co composition and the primary crystallization of Sm_5Co_2 is shown in Fig. 3e in a Sm–29Co sample. Micrographs of the heat-treated Sm–22Co (annealed at 500 °C for 45 days) specimen is given in Fig. 3c. The peritectic formation of the Sm_5Co_2 phase is confirmed by the BSE image of the Sm–27Co specimen reported in Fig. 3d, where the Sm_3Co primary crystals surrounded by the Sm_5Co_2 phase and the (Sm_5Co_2–$SmCo_2$) eutectic mixture can be observed. Micrograph of Sm–38Co alloy showing a nearly pure eutectic formed by Sm_5Co_2 (gray phase) and $SmCo_2$ (black phase) is reported in Fig. 3f.

4. Conclusions

The revised version of Sm–Co phase diagram on the Sm-rich side is proposed. More than 23 Sm–Co alloys were prepared and characterized. Only the use of slow heating/cooling rates for the DSC analysis makes it possible to clarify the relationship between Sm_3Co phase and different allotropic forms of Sm. The effect of crucibles has been highlighted. The existence of the Sm_3Co, Sm_5Co_2 and $SmCo_2$ binary phases has been verified and the temperatures of five invariant reactions have been determined.

Acknowledgements

Financial support from the China Scholarship Council is gratefully acknowledged. The authors wish to acknowledge the technical assistance of Mr. Enrico Puzo of Genoa University.

References

[1] D. Goll, H. Kronmüller, Naturwissenschaften 87 (2000) 423–438.
[2] J. Fiddler, T. Schrefl, S. Hoefinger, M. Hajduga, J. Phys.: Condens. Matter 16 (2004) 455–470.
[3] K. Kumar, J. Appl. Phys. 63 (1988) R13–R57.
[4] W. Tang, Y. Zhang, G.C. Hadjipanayis, Z. Metallkd. 93 (2002) 1002–1008.
[5] W. Ge, C. Wu, Y. Chuang, Z. Metallkd. 84 (1993) 165–169.
[6] L. Cataldo, A. Lefever, F. Ducret, M.-Th. Cohen-Adad, C. Allibert, N. Valignat, J. Alloys Compd. 241 (1996) 216–223.
[7] M.F. de Campos, F.J.G. Landgraf, J. Phase Equilib. 21 (2000) 443–446.

[8] A.S. van der Goot, K.H.J. Buschow, J. Less-Common Met. 14 (1968) 323–328.
[9] K.H.J. Buschow, F.J.A. Den Broeder, J. Less-Common Met. 33 (1973) 191–201.
[10] Y. Khan, Acta Crystallogr. Sect. B: Struct. Sci. 30 (1974) 861–864.
[11] K.L. Williams, R.W. Bartlett, P.J. Jorgensen, J. Less-Common Met. 37 (1974) 174–176.
[12] Y. Khan, Z. Metallkd. 65 (1974) 489–495.
[13] J.M. Moreau, D. Paccard, Acta Crystallogr. B32 (1976) 1654–1657.
[14] S. Derkaoui, C.H. Allibert, J. Less-Common Met. 154 (1989) 309–315.
[15] H. Stadelmaier, B. Reinsch, G. Petzow, Z. Metallkd. 89 (1998) 114–118.
[16] W.J. Boettinger, U.R. Kattner, K.-W. Moon, J.H. Perepezko, DTA and heat-flux DSC Measurements of Alloy Melting and Freezing, Natl. Inst. Stand. Technol., Spec. Publ. Washington, 2006.
[17] E.A. Leon-Escamilla, J.D. Corbett, J. Alloys Compd. 206 (1994) L15–L17.
[18] T.B. Massalski, H. Okamoto, Binary Alloy Phase Diagrams, 2nd ed., ASM International, OH, 1990.
[19] B.J. Beaudry, K.A. Gschneidener, in: G.J. McCarthy, J.J. Rhyne (Eds.), The Rare Earths in Modern Science and Technology, Plenum Press, New York, 1978, pp. 303–307.
[20] F.H. Spedding, J.J. Hanak, A.H. Daane, J. Less-Common Met. 3 (1961) 110–124.
[21] P.G. Mardon, C.C. Koch, Scripta Metall. 4 (1970) 477–483.
[22] B.J. Beaudry, P.E. Palmer, J. Less-Common Met. 34 (1974) 225–231.
[23] K.H.J. Buschow, A.S. van der Goot, J. Less-Common Met. 18 (1969) 309–311.
[24] O. Greis, P. Knappe, H. Muller, J. Solid State Chem. 39 (1981) 49–55.